Subwavelength imaging with quantum metamaterials

Ki Youl Yang,[*] Vincenzo Giannini, Alexey O. Bak, Hemmel Amrania, Stefan A. Maier, and Chris C. Phillips[†]
Experimental Solid State Group, Department of Physics, Imperial College London, London SW7 2AZ, United Kingdom
(Received 29 March 2012; published 14 August 2012)

We study the potential of a novel "quantum metamaterial" for subwavelength imaging applications in the midinfrared. Because the layers that comprise the metamaterial have in-plane and out-of-plane dielectric responses that are determined by different physical mechanisms (Drude free electron response and quantized electronic transitions, respectively), their resonances are polarization sensitive and can be designed independently. The result is a negatively refracting anisotropic effective medium with losses, described by the figure of merit, FOM $=$ Re($k_\perp$)/Im($k_\perp$) ~ 200 ($k_\perp$ is the wave vector), that are significantly lower than metamaterials based on classical layered systems. We find that, with sample design parameters that are realistically achievable with conventional epitaxy technologies, it is possible to obtain negative refraction for all incident angles, and finite element modeling studies indicate that these structures can function as so-called "hyperlenses," offering low-loss $\sim\lambda/13$ spatial resolution at mid-IR wavelengths of $\lambda \sim 10\ \mu$m.

DOI: 10.1103/PhysRevB.86.075309 PACS number(s): 78.20.Bh

I. INTRODUCTION

The concept of negative refraction has been known for several decades,[1] but only recently has it been realized that such materials offered the possibility of obtaining a "perfect" lens[2] capable of imaging below the diffraction limit. Advances in plasmonics[3] and in fabrication techniques[4] have generated significant interest in metamaterials, and a range of subwavelength resolution imaging[5–10] experiments have been reported. So-called "double negative" metamaterials ($\varepsilon, \mu \leqslant 0$) have also been experimentally demonstrated, and their operating regime has been shifted from microwave to visible frequencies.[11,12]

However, these implementations face technical challenges, typically high absorption and complexity of fabrication. Due to the nature of the resonances, high losses are induced within the material, thereby making it difficult to study negative refraction phenomena.

Anisotropic materials with $\varepsilon_\parallel > 0$ and $\varepsilon_\perp < 0$, where $\varepsilon_\parallel$ and $\varepsilon_\perp$ are the components of the permittivity parallel and perpendicular to the material surface, respectively, refract light such that, for transverse magnetic (TM) beams, the wave vector is deflected in the usual (i.e., positive) direction, but the Poynting vector is refracted negatively for all incident angles.[13,14] In the case of TM waves, these materials show negative refraction without the need for both negative electric and negative magnetic permittivity and permeability, and without needing absorption resonances. Hence, they can exhibit lower losses and they also offer simpler fabrication methods. They have also shown promising possibilities of subwavelength resolution imaging.[14,15]

Here we study a layered material where the $Al_{0.3}Ga_{0.7}As$/GaAs layers are not only both thin compared with the optical wavelength, but also the potential wells formed by the GaAs layers are thin enough to form quantum wells (QWs) that confine the electrons into a two-dimensional layer whose dielectric response can then be tailored using quantum-mechanical techniques.

II. QUANTUM METAMATERIAL DESIGN CONSIDERATIONS

While the $Al_{0.3}Ga_{0.7}As$ layers are isotropically dielectric [$\varepsilon_{B,\perp} = \varepsilon_{B,\parallel} = 9.65$ (Refs. 16 and 17)], in the quantum wells, the in-plane (x-y) electric fields see a Drude dielectric response, $\varepsilon_{QW,\parallel}$, determined by the density and mobility of the free electrons doped into the structure, but the perpendicular (z) field components see a QW intersubband transition (ISBT) dielectric response, $\varepsilon_{QW,\perp}$, characteristic of a fully quantized two-dimensional electron system. The extra degrees of freedom in the design of these "quantum metamaterials" allows improved performance to be designed into the structure.[16,17]

The ISBTs occur between two electron subbands. The electrons in these bands are free to move in the QW plane, so they have parabolic in-plane dispersion curves, but the two curves in the different subbands are parallel to each other, so whatever the electron in-plane momentum, the electronic transition occurs at the same energy [Fig. 1(b)]. This, combined with strong electron-electron correlation effects, generates a sharply peaked single-Lorentzian-like absorption spectrum [Fig. 1(c)].

The Lorentzian peak energy and strength are determined by the QW width and electron density, respectively, and they can be tuned independently of the in-plane dielectric response. In these quantum metamaterials, the ISBT can be thought of as playing a role analogous to the electromagnetic resonances in conventional metamaterials. However, there is the added twist that each layer in these structures inherently exhibits an extreme version of optical anisotropy that has a quantum-mechanical and not just a geometrical origin; the electron motion is completely free in one direction (x-y), and completely bound in the other (z).

III. DESIGN PARAMETERS

For definiteness we consider an $Al_{0.3}Ga_{0.7}As$/GaAs multiple quantum-well structure. We fix the $Al_{0.3}Ga_{0.7}As$ barrier width at $d_B = 8$ nm and consider a range of GaAs QW

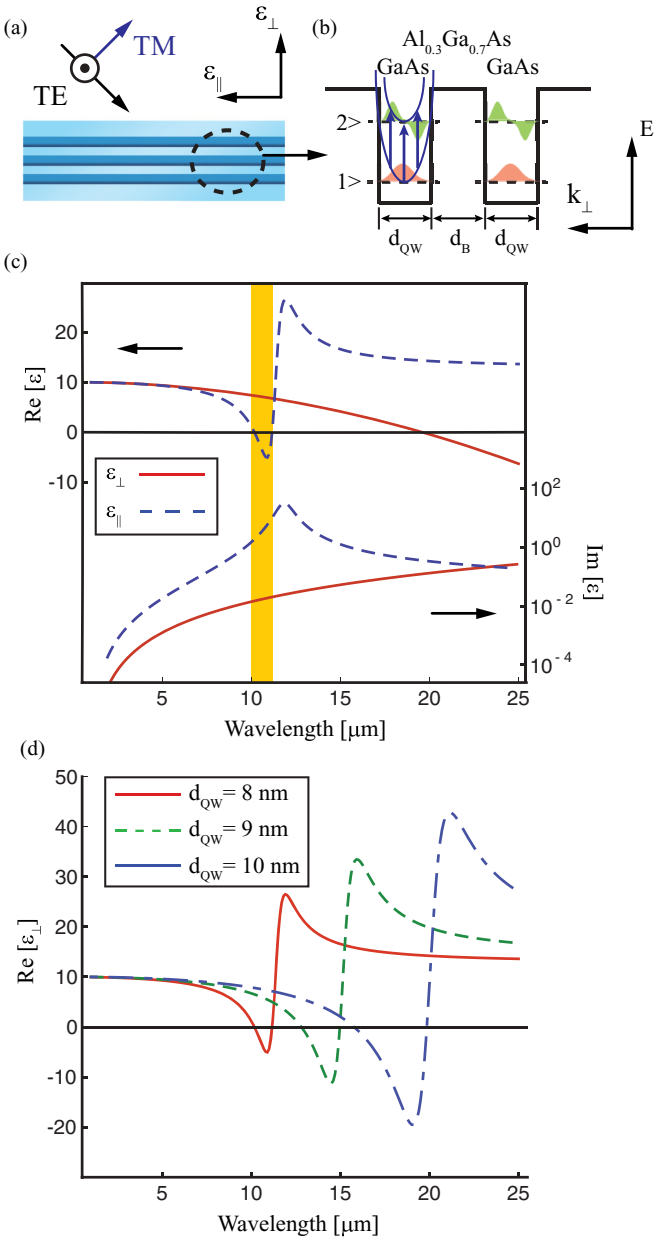

FIG. 1. (Color) (a) Geometry of the quantum metamaterial and orientation of the polarized electric fields. (b) Schematic of the electronic energy level structure in each QW layer, showing the "intersubband transition" between the confined electron states that generates the tunable peak in the dielectric response. (c) Real and imaginary part of the effective permittivity $\varepsilon_{\mathrm{QW},\parallel}$ and $\varepsilon_{\mathrm{QW},\perp}$ of a quantum well with 8 nm GaAs thickness. (d) Real part of $\varepsilon_{\mathrm{QW},\perp}$ dependence on the GaAs layer thickness.

widths (d_{QW}) that generate ISBT energies corresponding to the midinfrared region, i.e., comparable to the plasma frequencies for typical semiconductor doping densities.[16–18] The dielectric response functions are calculated as in Refs. 16–18 with the input parameters of Table I.

In the case of the 8 nm QW, the sheet electron density corresponds to a bulk donor density in the well of 3.6×10^{18} cm^{-3}, i.e., within 10% of the effective donor solubility limit of $\sim 4 \times 10^{18}$ cm^{-3} for molecular-beam-epitaxial (MBE) growth. For the wider QWs the sheet carrier density is chosen

TABLE I. Quantum-well parameters used to compute the dielectric responses of the multi-quantum-well component of the quantum metamaterial slabs.

d_{QW} (nm)	z_{12} (nm)	E_{12} (meV)/(μm)	n_s (cm^{-2})	E_F (meV)
8	2.117	124/10.0	2.88×10^{12}	103
9	2.382	98/12.7	2.45×10^{12}	88
10 nm	2.646	80/15.6	2.0×10^{12}	71

to give a Fermi energy that is 90% of the ISBT energy, E_{12}, so that, within typical MBE growth tolerances, the second subband will be sure to be empty.

Because the ISBT energy is independent of the electron in-plane wave vector, the absorption peak is largely temperature independent. The calculations here assumed all the carriers are in the lowest subband, but even at room temperature, e.g., in the case of the 8 nm QW design, the absorption peak intensity will drop by $<10\%$ as a result of thermal excitation of electrons into the second subband.

The QW ISBT energies and transition dipole strengths (z_{12}) were calculated using a standard numerical QM model as described elsewhere.[17] Realistic electron scattering rates, corresponding to full-width-half-maximum ISBT linewidths of 4% of E_{12} were used.

IV. QUANTUM METAMATERIAL DIELECTRIC RESPONSES

Figure 1(c) shows the real and imaginary parts of the effective permittivity for the $d_{\mathrm{QW}} = 8$ nm nanostructure. The shaded region to the low-energy side of the ISBT peak is that of negative response for a TM-polarized incident field.[16–18]

Figure 1(d) shows the frequency dependence of Re[$\varepsilon_\perp$] as a function of QW width, illustrating the way in which, in wider QWs, the increase in transition dipole generates more pronounced regions of negative response as z_{12}, and hence the absorption strength increases and the ISBT narrows.

Note that the dielectric response is dominantly determined by d_{QW} in these nanostructures, and potentially this offers a more reproducible way of generating negative refraction because, in MBE, layer thicknesses are typically easier to control accurately than doping densities.

The $d_{\mathrm{QW}} = 8$ nm QW design has an in-plane dielectric response that is positive (Re[$\varepsilon_{\mathrm{QW},\parallel}$] > 0) for the majority of the spectrum, and only goes negative for wavelengths longer than the $\lambda \sim 18$ μm value corresponding to the plasma frequency of the quasi-two-dimensional electron gas (Q2DEG) layer.

Figure 2(a) shows the figure of merit, defined as FOM = Re($k_\perp$)/Im($k_\perp$), and the TM absorption coefficient, $\alpha = 2$ Im($k_\perp$) for the $d_{\mathrm{QW}} = 8$ nm design. These were deduced from the dielectric functions of Fig. 1(c) ($d_{\mathrm{QW}} = 8$ nm), which in turn were calculated from the effective medium approximation[16–18] as a function of the wavelength at different incidence angles. Interestingly, we found that the figure of merit (FOM) can be larger than 200 in the negative refraction region, i.e., roughly an order of magnitude larger than reported for structures with geometrically engineered anisotropy.[13]

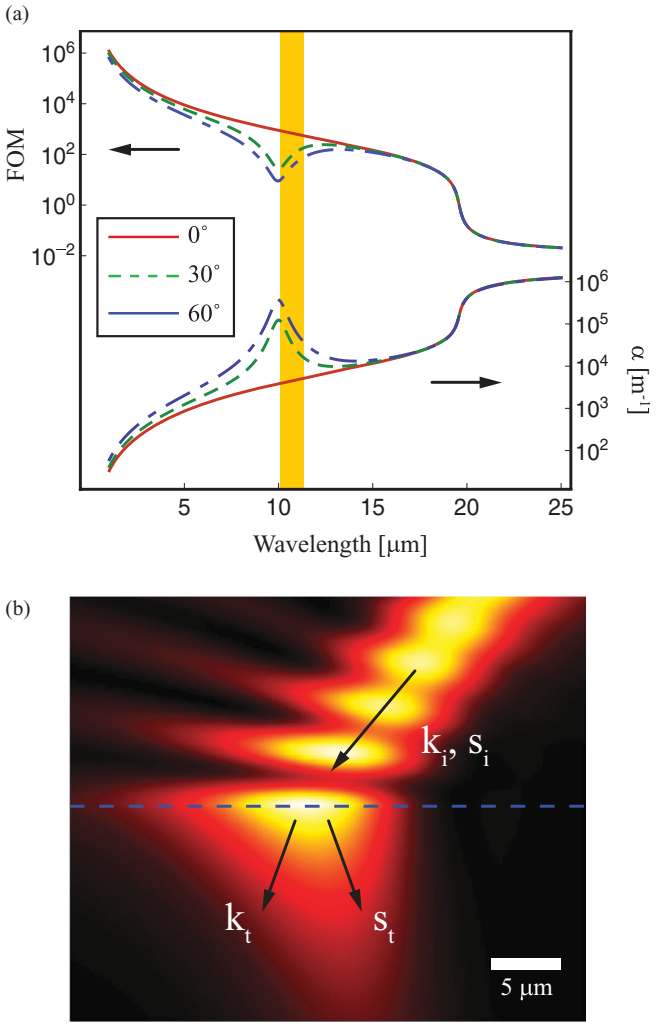

FIG. 2. (Color) (a) Calculation of the absorption coefficient α and FOM for a TM incident wave, as a function of the wavelength for the quantum metamaterial of Fig. 1(a). (b) Near-field (|Hy|) calculation of a monochromatic TM Gaussian beam across the air/metamaterial interface, $\lambda = 10.46\ \mu$m. The arrows show the direction of the Poynting vector of the transmitted beam, S_t, which indicates the negative refraction in the metamaterial, and the associated wave vector, k_t.

V. NEGATIVE REFRACTION CHARACTERISTICS

Figure 2(b) shows numerical calculations of the refraction across the air/metamaterial interface [of Fig. 1(a)] for a TM-polarized Gaussian beam computed with a standard finite-difference time-domain (FDTD) method at a wavelength ($\lambda = 10.46\ \mu$m) where the $d_{QW} = 8$ nm structure has a negative out-of-plane dielectric response. We calculate |Hy| on the x-z plane with the wave beam impinging at $\Theta = +40^\circ$ with respect to the layer normal. The incident beam is then refracted at the air/metamaterial interface and propagates at an angle of $\Theta = -11^\circ$ through the metamaterial structure. Notice that the refracted beam has an opposite propagation direction with respect to the incident beam, i.e., it is refracting negatively.

The quantum metamaterial slab is an effective medium with, in the frequency range where $\varepsilon_\perp < 0$ and $\varepsilon_\parallel > 0$, a hyperbolic dispersion characteristic (Fig. 3), given by

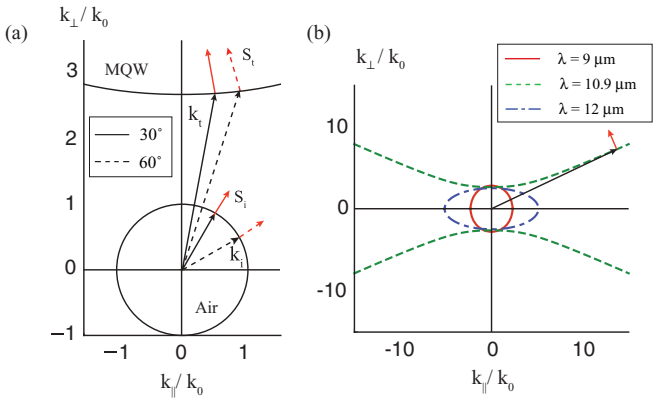

FIG. 3. (Color) (a) Isofrequency dispersion curves comparing the dispersion in air and in the $d_{QW} = 8$ nm quantum metamaterial slab of Fig. 1, at the wavelength $\lambda = 10.49\ \mu$m, where the refraction modeling in Fig. 2 took place. k_i and k_t represent the incident and transmitted wave vectors, respectively, and S_i and S_t are the respective energy flows for incident beam angles of 30° (solid lines) and 60° (dashed lines). (b) Isofrequency dispersion curves for the quantum metamaterial slab showing the transition from near-isotropic to hyperbolic to uniaxial dispersion characteristics as the wavelength is tuned through the negative response region corresponding to the electronic ISBT transitions in the quantum wells. The arrow denotes the propagation direction of the dominant $k_\parallel/k_0 \sim 13.8$ spatial frequency components in the image. These propagate as "nondiffracting rays," almost normal to the metamaterial layers.

$$\frac{k_\parallel^2}{\varepsilon_\parallel} + \frac{k_\perp^2}{\varepsilon_\perp} = k_0^2, \tag{1}$$

where the effective medium dielectric response components $\varepsilon_\perp$ and $\varepsilon_\parallel$ are related to those of the QWs ($\varepsilon_{QW,\perp}$ and $\varepsilon_{QW,\parallel}$) and the barriers ($\varepsilon_{B,\perp}$ and $\varepsilon_{B,\parallel}$), by

$$\varepsilon_\parallel = \frac{(d_{QW}\varepsilon_{QW,\parallel} + d_B\varepsilon_{B,\parallel})}{d_{QW} + d_B}, \tag{2}$$

$$\varepsilon_\perp = \frac{(d_{QW} + d_B)\varepsilon_{QW,\perp}\varepsilon_{B,\perp}}{(d_B\varepsilon_{QW,\perp} + d_{QW}\varepsilon_{B,\perp})}. \tag{3}$$

The hyperbola's asymptotes are given by

$$k_\perp = \pm\sqrt{\left|\frac{\varepsilon_\parallel}{\varepsilon_\perp}\right|}k_\parallel. \tag{4}$$

The high spatial frequency components of the image, whose group velocities are normal to the dispersion curves' asymptotes, are "beamed" through the slab along a so-called "cone of resonance." This system has been studied previously,[15] for the case where the two components of the metamaterial consist of materials that are themselves isotropic but with dielectric responses of the opposite sign. If the layer thicknesses are chosen so the $\varepsilon_\parallel$ response is small (so-called epsilon-near-zero metamaterials), then the dispersion hyperbola can be made to flatten out, and these cones of resonance collapse into a single ray that travels through the slab almost undistorted by diffraction.

Taking the expression for the dispersion curve and substituting appropriate values for the dielectric response components corresponding to a free-space wavelength of 10.9 μm, gives a

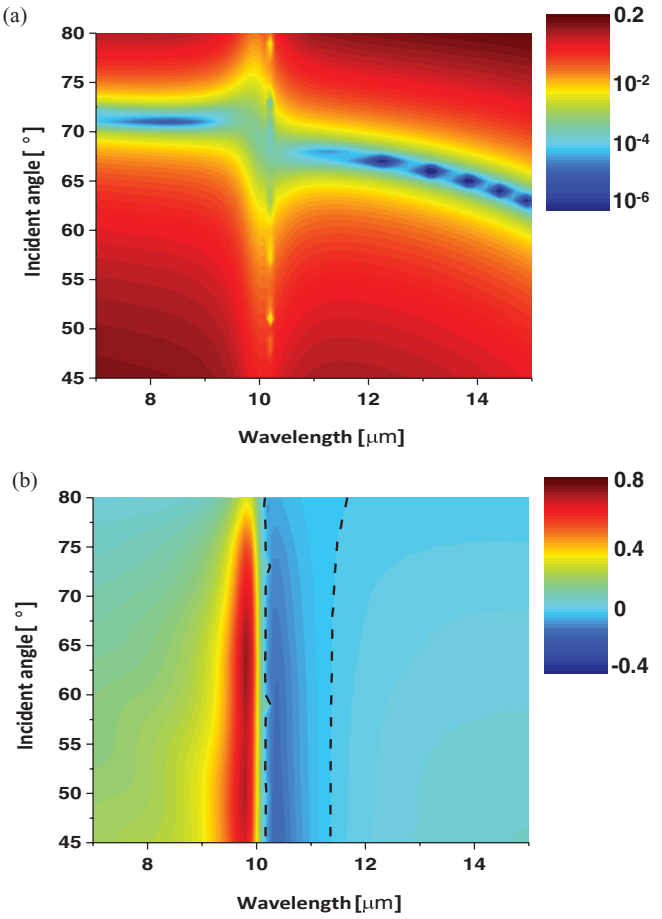

FIG. 4. (Color) (a) Logarithmic plot of the TM beam reflectivity of the $d_{QW} = 8$ nm quantum metamaterial slab as a function of wavelength and incident angle, Θ, to the sample normal. Note the pronounced discontinuity in the $\sim 10.1\ \mu m < \lambda < \sim 11.4\ \mu m$ spectral region where the negative refraction occurs. (b) Contour plot of the in-plane component of the energy flow inside the quantum metamaterial slab, as a fraction of the in-plane component of the energy flow in the incident beam. Note the negative region appearing at all incident angles in the ($\sim 10.1\ \mu m < \lambda < \sim 11.4\ \mu m$) spectral region where $\varepsilon_{QW,\perp}$ for the QWs is negative.

ray propagation direction,

$$\frac{\partial k_\perp}{\partial k_\parallel} = -\frac{\varepsilon_\parallel}{\varepsilon_\perp}\frac{k_\parallel}{k_\perp}$$

of -13°, compared with the -11° from the FDTD simulation, the difference being due to the fact that the latter assumes an incident beam with a Gaussian intensity profile, and a corresponding spread in $k_\parallel$ values.

VI. QUANTUM METAMATERIAL REFLECTIVITY CHARACTERISTICS

The anisotropic nature of the quantum metamaterial is also evident in the angular dependence of its reflectivity [Fig. 4(a)], where a pronounced discontinuity occurs at the $\lambda \sim 10\ \mu m$ spectral region where the negative refraction sets in, accompanied by an angle-dependent reflectivity minimum at longer wavelengths. Plotting the in-plane component of the energy flow in the beam inside the metamaterial [Fig. 4(b)] also clearly illustrates the negative sign of the refracted component in the quantum metamaterial at all incident angles.

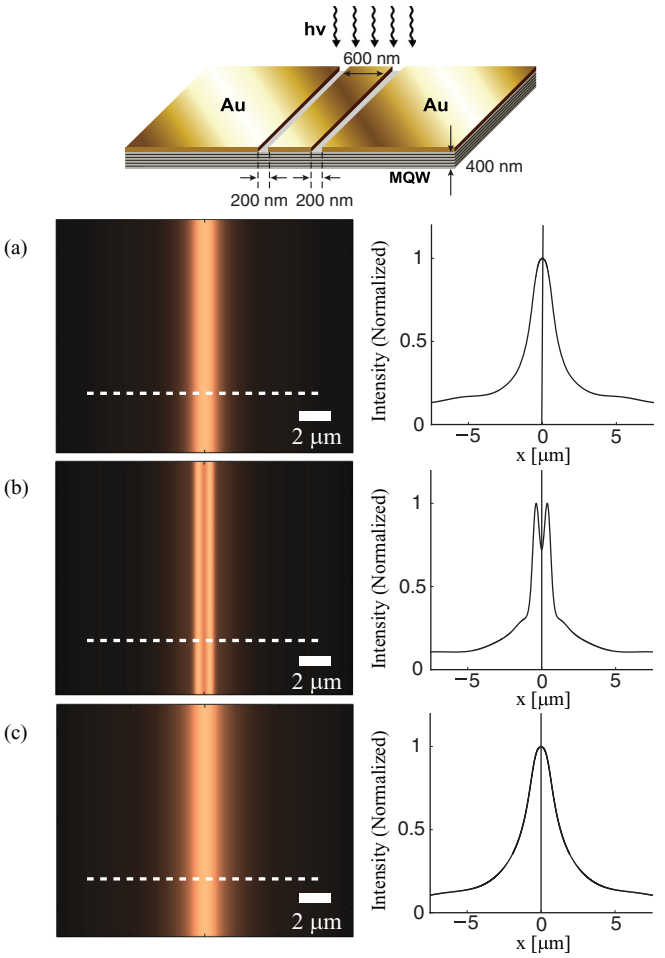

FIG. 5. (Color) Left: (a) |Hy| near-field image at the air/metamaterial interface at $\lambda = 9\ \mu m$, (b) at 10.9 μm, and (c) at 10.9 μm for a dielectric substrate with $n = 1.5$. Right: intensity plots along the dashed lines. Note the super-resolved image at (b) when the wavelength is tuned to the spectral region where the negative refraction occurs. The inset shows an illustration of the imaging system, made with a 300-nm-thick gold film with two slits of 200 nm separated (center to center) by 800 nm. The film is deposited on a 0.4-μm-thick quantum-metamaterial substrate composed of $d_{QW} = 8$ nm quantum wells and $d_B = 8$ nm barrier slabs as in Fig. 2.

VII. SUB WAVELENGTH IMAGING

To explore the potential of these structures for subwavelength imaging we conducted a numerical simulation of a subdiffraction-limited imaging experiment. The object to be imaged consisted of a 300-nm-thick gold mask film, with two 200-nm-wide slits etched in it, with their centers 800 nm apart. The imaging slab consisted of 400 nm of quantum metamaterial, with $d_B = 8$ mn barrier slabs and $d_{QW} =$ 8-nm-wide wells as detailed above.

The structure is illuminated, at normal incidence, with a TM-polarized mid-IR plane wave. Each aperture generates

the same single diffraction pattern, containing high in-plane wave-vector components (evanescent light), which carry the high-resolution information through to the image plane.[2,15] Figure 5(a) shows how the field |Hy| at the image plane (i.e., the lower metamaterial-air interface) evolves as the wavelength of the impinging field is tuned from outside [$\lambda = 9\ \mu$m, Fig. 5(a)] to inside [$\lambda = 10.9\ \mu$m, Fig. 3(a)] the negatively refracting spectral region. For comparison we also show |Hy| when the imaging slab is composed of a uniform simple dielectric with refractive index $n = 1.5$ [Fig. 5(c)].

We can see from Fig. 5(b) that the images of the slits are clearly distinguishable only in the $\lambda = 10.9\ \mu$m regime where the negative refraction characteristic occurs. In this case the quantum metamaterial enables structure in the image that is more than ten times smaller than the wavelength of the incident light ($\lambda/\text{gap} = 10.9\ \mu\text{m}/0.8\ \mu\text{m} \sim 13.75$) to be reproduced.[15]

Plotting out the dispersion relation [Fig. 4(b)] shows how this can be understood in the "nondiffracting ray" picture.[15] The 800-nm slit separation results in a set of image spatial frequencies centered at $k_{\parallel}/k_0 \sim 13.8$, i.e., well along the asymptotes of the hyperbola, that propagate almost normally to the layers.

In contrast to previous ε-near-zero metamaterials however, these rays are propagating with a polarization that is only weakly coupled to the ISBTs. This dramatically reduces the losses, giving the high FOM that means that ~45% of the light is transmitted through the device.

The intrinsic optical anisotropy that is introduced by going to layers thin enough to confine the electrons quantum mechanically has allowed us to generate a hyperlens where the required dispersion characteristics come not from a zero in the $\varepsilon_{\parallel}$ response, but a divergence in the $\varepsilon_{\perp}$ response, and where the extra design flexibility allows polarization-dependent tailoring of the response in a way that allows losses to be curtailed.

VIII. CONCLUDING REMARKS

To conclude, we have proposed an imaging system based on a quantum metamaterial composed of uniformly doped QW layers. A careful design of the structure allows the ISBT transition to be spectrally separated far from the plasmon Q2DEG resonance; this provides a negative refraction zone that is polarization dependent and energy tunable, and offers with lower losses and hence an improved FOM (>200). In addition, FDTD numerical simulations demonstrate negative refraction along an air/metamaterial interface, and a subdiffraction-limited image of a structure that is ten times smaller than the incident wavelength.

In common with other subwavelength imaging studies, the subwavelength resolution is only available in the near field. That is to say that the quantum metamaterial slab effectively transfers the field distribution at one of its faces to the other, with a minimal loss of fidelity.[15] This facility is expected to be particularly useful for IR chemical imaging of live cells[19] where a custom-designed quantum metamaterial layer could serve as a barrier between the wet nutrient-carrying environment needed to support cell life, and a dry side where the field is present in an environment suitable for subwavelength imaging with probe-based techniques such as scattering-scanning near-field optical microscopy.

These results imply a potential for "hyper lenses" based on these new quantum metamaterials to offer super-resolved IR images in a range of systems that are of interest across the life sciences and biomedical imaging.

ACKNOWLEDGMENTS

This work was sponsored by the Engineering and Physical Sciences Research Council (EPSRC). V.G. acknowledges funding from the EU through the Marie Curie IEF programme.

*Present address: Thomas J. Watson Laboratory, California Institute of Technology, Pasadena, CA 91125.
†Corresponding author: chris.phillips@imperial.ac.uk

[1] V. Veselago, Phys. Usp. **10**, 509 (1968).
[2] J. Pendry, Phys. Rev. Lett. **85**, 3966 (2000).
[3] V. Giannini, A. I. Fernandez-Dominguez, S. C. Heck, and S. A. Maier, Chem. Rev. **111**, 3888 (2011).
[4] D. R. Smith and N. Kroll, Phys. Rev. Lett. **85**, 2933 (2000).
[5] N. Fang, H. Lee, C. Sun, and X. Zhang, Science **308**, 534 (2005).
[6] V. Podolskiy and E. Narimanov, Opt. Lett. **30**, 75 (2005).
[7] H. Liu and K. Webb, Opt. Lett. **33**, 2568 (2008).
[8] X. Zhang and Z. Liu, Nat. Mater. **7**, 435 (2008).
[9] S. Thongrattanasiri and V. Podolskiy, Opt. Lett. **34**, 890 (2009).
[10] S. C. Kehr, Y. M. Liu, L. W. Martin, P. Yu, M. Gajek, S. Y. Yang, C. H. Yang, M. Wenzel, R. Jacob, H. G. von Ribbeck, M. Helm, X. Zhang, L. Eng, and R. Ramesh, Nat. Commun. **2**, 249 (2011).
[11] G. Dolling, M. Wegener, C. M. Soukoulis, and S. Linden, Opt. Lett. **32**, 53 (2007).
[12] S. P. Burgos, R. De Waele, A. Polman, and H. A. Atwa-ter, Nature Mater. **9**, 407 (2010).
[13] A. J. Hoffman, L. Alekseyev, S. Howard, K. J. Franz, D. Wasserman, V. A. Podolskiy, E. E. Narimanov, D. L. Sivco, and C. Gmachl, Nature Mater. **6**, 946 (2007).
[14] A. Fang, T. Koschny, and C. M. Soukoulis, Phys. Rev. B **79**, 245127 (2009).
[15] A. Salandrino and N. Engheta, Phys. Rev. B **74**, 075103 (2006).
[16] J. Plumridge and C. C. Phillips, Phys. Rev. B **76**, 75326 (2007).
[17] J. R. Plumridge, R. J. Steed, and C. C. Phillips, Phys. Rev. B **77**, 205428 (2008).
[18] M. Zaluzny and C. Nalewajko, Phys. Rev. B **59**, 13043 (1999).
[19] H. Amrania, A. P. McCrow, M. R. Matthews, S. G. Kazarian, M. K. Kuimova, and C. C. Phillips, Chem. Sci. **2**, 107 (2011).